



Docking to flexible nicotinic acetylcholine receptors: A validation study using the acetylcholine binding protein

Tommy Sander^a, Anne T. Bruun^b, Thomas Balle^{a,*}

^a Department of Medicinal Chemistry, Faculty of Pharmaceutical Sciences, University of Copenhagen, Universitetsparken 2, DK-2100 Copenhagen, Denmark

^b H. Lundbeck A/S, Ottilavej 9, DK-2500 Valby, Denmark

ARTICLE INFO

Article history:

Received 2 June 2010

Received in revised form 28 July 2010

Accepted 17 August 2010

Available online 29 September 2010

Keywords:

Protein flexibility

Molecular docking

Ensemble generation

Nicotinic

Acetylcholine receptors

nAChR

Acetylcholine binding protein

AChBP

ABSTRACT

Computational docking to nicotinic acetylcholine receptors (nAChRs) and other members of the Cys-loop receptor family is complicated by the flexibility of the so-called C-loop. As observed in the large number of published crystal structures of the acetylcholine binding protein (AChBP), a structural surrogate and homology modeling template for the nAChRs, the conformation of this loop is controlled by the ligand present in the binding pocket. As part of the development of a protocol for unbiased docking to the nAChRs, we here present the results of docking of ligands with known binding modes to an AChBP ensemble with systematic variations in C-loop closure generated via a series of targeted geometry optimizations. We demonstrate the ability to correctly predict binding modes for 12 out of 15 ligands and induced degrees of C-loop closure for 14 out of 15 ligands. Our approach holds a promising potential for structure based drug discovery within nAChRs and related receptors.

© 2010 Elsevier Inc. All rights reserved.

1. Introduction

Nicotinic acetylcholine receptors (nAChRs) constitute a pharmaceutically important class of pentameric ligand-gated ion channels called Cys-loop receptors, to which also the GABA_A, glycine and 5-HT₃ receptors belong [1]. The rational design of new ligands and application of virtual screening towards these receptors is hampered by the lack of a high-resolution X-ray structure of the ligand-binding site of the nAChRs. To date, the only nAChR structures available are the 4 Å electron microscopy of the muscle type nAChR from *Torpedo marmorata* [2] and the X-ray structure of the N-terminal part of the mouse α_1 monomer [3]. Augmented with structural information from the acetylcholine binding protein (AChBP) isolated primarily from the freshwater snails *Lymnaea stagnalis* (Ls) and *Aplysia californica* (Ac) [4–16], these structures form the basis for homology models of nAChRs and other Cys-loop receptors [17]. The AChBP is homologous to the ligand binding extra-cellular domain of the nAChR and, equally importantly, binds key nicotinic ligands such as ACh, nicotine, epibatidine, and methyllycaconitine (MLA) (structures shown in Table 1). Hence, they are regarded as functional and structural surrogates of the

nAChR [9,18], and apart from being used extensively as templates for the construction of homology models they have also been used directly in virtual screening with the purpose of discovering novel nAChR ligands [15]. Until now 26 structures of the AChBP in the apo form, in complex with buffer molecules, toxins and small molecule nicotinic agonists, partial agonists, antagonists and allosteric modulators have been deposited in the Protein Data Bank (PDB) [19]. Despite low overall sequence identity to nAChRs [20] the ligand-binding site is much better conserved and the protein thus provides detailed insights into the protein–ligand interactions of nicotinic ligands. An interesting observation from the many AChBP structures is the large flexibility of the binding site, in particular originating from the 10 to 12 residue hairpin shaped C-loop being able to move away from, or close in on, the site to accommodate differently sized ligands (Fig. 1). Comparing AChBP structures co-crystallized with agonists to those with antagonists it is clear that agonists stabilize full C-loop closure while antagonists hold the loop in an open conformation. Several studies have indicated C-loop closure to be involved in the receptor activation process which eventually leads to opening of the ion channel in nAChRs [21–24]. Obviously, the C-loop flexibility has a large impact on the size and shape of the binding pocket, and a prerequisite for successful application of structure based design, automated docking and virtual screening to nAChRs and other Cys-loop receptors is the ability to account for this flexibility.

* Corresponding author. Tel.: +45 35336409; fax: +45 35336040.

E-mail address: tb@farma.ku.dk (T. Balle).

Table 1
Ligand names, structures, AChBP complex details, binding affinities, and cross-docking results.

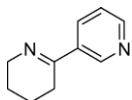
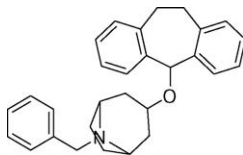
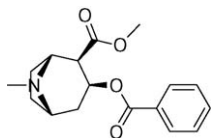
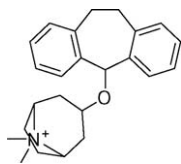
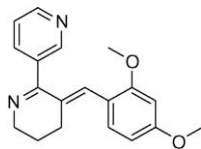
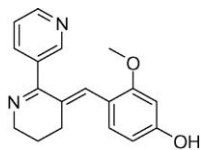
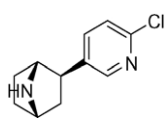
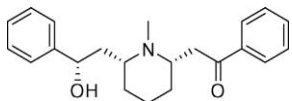
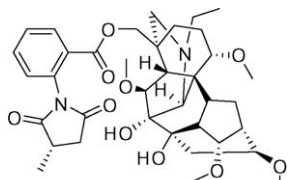
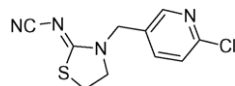
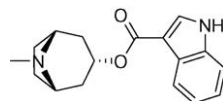
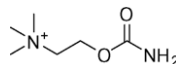
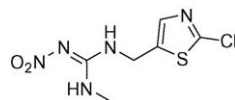
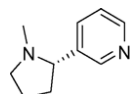
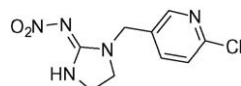
Ligand			Structure	Sp.	Affinity ^a		Self-docking ^b		Cross-docking ^c		
PDB code	Closure	Ref.			<i>pK_i/pK_D</i>	Ref.	Gscore	RMSD	Gscore	RMSD	PDB
Ac-AChBP											
	Anabaseine			Ac	<6	[51]	−10.43	1.2 Å	−11.13	1.1 Å	2byq
2wnl	12.1 Å	[16]		Ls	6.6	[51]	–	–	−11.61	0.8 Å	2zjv
	BDSAO ^d			Ac	6.0	[15]	−7.79	2.2 Å	−7.79	2.2 Å	2w8g-DE
2w8g	18.3–19.8 Å	[15]		Ls	7.0	[15]	–	–	None	–	–
	Cocaine			Ac	5.7	[11]	−10.24	0.8 Å	−11.08	1.7 Å	2wnc
2pgz	14.0 Å	[11]		Ls	–		–	–	None	–	–
	DDSAO			Ac	6.3	[15]	−6.60	1.5 Å	−7.06	1.8 Å	2w8g-DE
2w8f	18.3 Å	[15]		Ls	7.2	[15]	–	–	None	–	–
	DMXBA			Ac	6.5	[51]	−11.83	0.5 Å	−12.31	0.9 Å	2wn9
2wnj	13.8 Å	[16]		Ls	7.7	[51]	–	–	−5.79	7.0 Å	2zju
	4-OH-DMXBA			Ac	8.5	[51]	−12.90	0.5 Å	−12.90	0.5 Å	2wn9
2wn9	13.9 Å	[16]		Ls	9.4	[51]	–	–	−6.18	8.1 Å	2zju
	Epibatidine			Ac	7.9	[52]	−10.46	0.4 Å	−10.46	0.4 Å	2byq
2byq	12.0 Å	[9]		Ls	9.8	[18]	–	–	−11.02	0.6 Å	1uw6
	Lobeline			Ac	9.5	[9]	−11.64	1.2 Å	−11.64	1.2 Å	2bys
2bys	12.3 Å	[9]		Ls	7.5	[9]	–	–	−5.01	6.6 Å	2zju
	MLA			Ac	8.6	[52]	−10.48	1.2 Å	−10.56	1.3 Å	2w8g-DE
2byr	18.2 Å	[9]		Ls	9.4	[52]	–	–	None	–	–

Table 1 (Continued)

Ligand			Structure	Sp.	Affinity ^a		Self-docking ^b		Cross-docking ^c		
PDB code	Closure	Ref.			<i>pK_i</i> / <i>pK_D</i>	Ref.	Gscore	RMSE	Gscore	RMSE	PDB
3c84	Thiacloprid	[14]		Ac	7.9	[14]	−6.50	0.2 Å	−6.74	0.5 Å	3c79
	11.7 Å		Ls	–	–	–	–	−7.48	1.3 Å	2zju	
2wnc	Tropisetron	[16]		Ac	6.32	[16]	−11.57	1.2 Å	−11.87	3.9 Å	2pgz
	14.1 Å		Ls	7.1	[16]	–	–	−4.48	7.8 Å	2zju	
Ls-AChBP											
1uv6	Carbamoylcholine	[5]		Ac	3.6	[52]	–	–	−9.23	2.0 Å	2wn9
	12.6 Å		Ls	5.3	[52]	−8.62	0.9 Å	−9.10	1.1 Å	1uw6	
2zjv	Clothianidin	[13]		Ac	–		–	–	−6.03	1.0 Å	3c79
	12.8 Å		Ls	5.14	[13]	−6.08	0.7 Å	−6.08	0.7 Å	2zjv	
1uw6	Nicotine	[5]		Ac	6.61	[52]	–	–	−9.71	1.2 Å	2byq
	12.4 Å		Ls	7.4	[18]	−10.73	0.3 Å	−10.73	0.3 Å	1uw6	
Ac and Ls-AChBP											
Ac: 3c79 Ls: 2zju	Imidacloprid	[14] [13]		Ac	7.2	[14]	−6.94	0.6 Å	−6.94	0.6 Å	3c79
	12.3 Å 15.1 Å		Ls	5.80	[13]	−6.83	0.2 Å	−7.65	0.7 Å	2zju	

^a Binding affinities given in the left column were measured by radioligand displacement or tryptophan fluorescence quenching studies as described in the citation specified in the right column.

^b Gscore and RMSD of the best Emodel scoring pose in its native receptor.

^c Best Gscore and corresponding RMSD in any receptor (*Ac* and *Ls* evaluated separately) when comparing the Gscores of the best Emodel pose in each receptor.

^d Best BDSAO docking result (shown) was obtained in the 2w8g-DE interface with the corresponding tautomer; RMSD compared to the native DE interface ligand structure.

Receptor flexibility in docking and virtual screening studies is traditionally handled by application of van der Waals (vdW) scaling to ligand and/or receptor atoms to allow closer contacts [25], or more directly, by modeling induced fit at the single residue level to sample rotameric states and allow selected residues to adapt optimally to the ligand [26]. However, these methods are often not appropriate for exploring effects of large-scale motions such as that observed for the AChBP. If the binding site, because of the protein backbone conformation, is too narrow for a bulky ligand to bind, no initial docking pose would be found for the subsequent side chain optimization in induced fit docking. Conversely, upon docking a small ligand to a spacious cavity, an induced fit optimization would not narrow the site by moving an entire protein domain, e.g. pulling an open C-loop in the AChBP inwards over the pocket. Protein flexibility at larger scales, i.e. loop or domain movements, is better handled by docking to conformational ensembles, either obtained by sampling techniques such as molecular dynamics (MD) [27–29] or normal mode analysis (NMA) [30–32], or from experimental sources if available [33].

We here present an evaluation study on a novel procedure for modeling large-scale motions using a series of targeted molecular mechanics geometry optimizations. It is based on AChBP structures

from *Ac* and *Ls* to allow for validation against experimentally determined structures. The study is centered on computational docking of 15 AChBP ligands to an ensemble of AChBPs with systematic variations in the degree of C-loop closure, and is divided into three stages:

- (1) A cross-validation study where all 15 small-molecule AChBP ligands are docked to an ensemble of experimentally determined AChBP structures to identify the best docking/scoring protocol, and to evaluate the prerequisite of the study, namely that the best scoring pose of a given ligand is obtained in a receptor with the correct degree of C-loop closure.
- (2) An ensemble generation stage aimed at generating a set of AChBP structures with systematic variations of C-loop closure from a single AChBP structure.
- (3) An ensemble docking stage where the 15 ligands are docked to the generated AChBP ensemble.

We demonstrate that the correct ligand–receptor pairs generally can be identified based on the docking score without *a priori* knowledge of the degree of C-loop closure induced by the ligand.

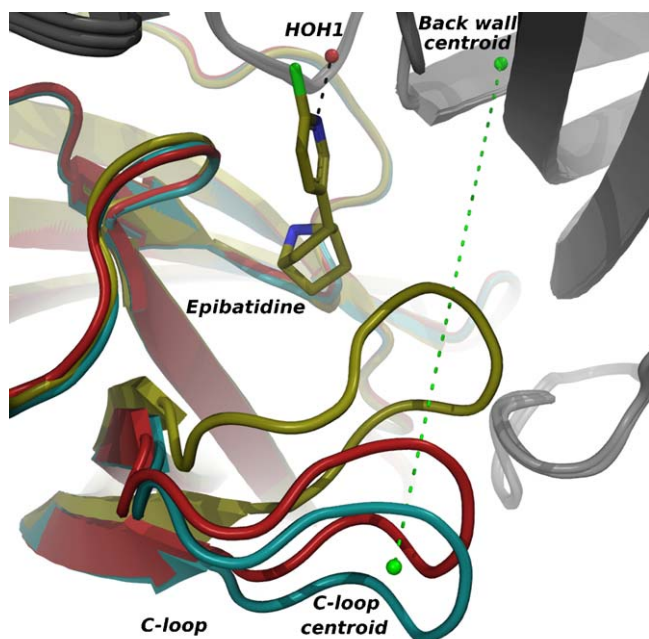


Fig. 1. Close-up view of the binding pocket of three AChBP structures with different degrees of C-loop closure, with epibatidine included to highlight the location of the binding site. Water molecule HOH1 (red sphere) and the two centroids (green spheres; see Section 2) defining the C-loop closure are shown in their positions in the 2byn structure. Complementary (–) subunits are colored in gray. Principal (+) subunit coloring: 2byn (teal), 2byr (ruby), and 2byq (gold). (Image generated with PyMOL [50]). (For interpretation of the references to color in this figure legend, the reader is referred to the web version of the article.)

2. Methods

2.1. General methods and definitions

All molecular modeling tasks were performed on Intel Xeon x86.64 processors, using the Schrödinger 2008 suite with Maestro 8.5 [34] for visualization, building and measuring purposes, Glide 5.0 [35–37] for docking, and MacroModel 9.6 [38] for molecular mechanics calculations. Slightly modified versions of the OPLS 2001 and 2005 force fields were used for docking and minimizations, respectively. The modification provided by Schrödinger ensured co-planarity of the nitroguanidine moiety of clothianidin and imidacloprid and as such corresponds to the OPLS force fields in the Schrödinger 2009 update 2 release. Binding free energy for water molecules was calculated with GRID [39,40] in the dimer interface between chains A and E of the apo structure (PDB code: 2byn) of the AChBP from *Ac* using the water probe and two planes per Å. (In the remainder of this paper, *Ac*-AChBP and *Ls*-AChBP are used to refer to the AChBP from *A. californica* and *L. stagnalis*, respectively.)

Residues are generally denoted with (+) or (–), indicating their position on the principal (i.e. C-loop contributing) or complementary subunit, respectively. RMSD comparisons between receptor structures are based on pocket residues only, which we define as the entire C-loop plus any residue within 5 Å of any ligand, excluding the structurally diverging F-loop (*Ac* residues T158–K173). Thus, for *Ac* the pocket residues are defined as residues (+) T91–S94, M126, K143–S150, Q184–D197, and (–) T36–Q38, Y55–R59, R79, I106–V108, M116–I118, and correspondingly for *Ls* as (+) A87–N90, S122, K139–H146, N181–D194, and (–) K34–I36, W53–T57, S75, L102–R104, L112–M114. The degree of C-loop closure is defined as the distance between the ‘C-loop tip centroid’ and the ‘back wall centroid’, where the former is the C α centroid of residues (+) Y188–C191 (*Ac*) or Y185–C188 (*Ls*), and the latter is on the (–) side between C α , C and O backbone atoms of E56 (*Ac*) or Q54 (*Ls*), and C α

of P119 (*Ac*) or P115 (*Ls*). The water molecule referred to as HOH1 throughout this study is defined as the water molecule, found in all published AChBP structures where waters are modeled into the electron density (i.e. all except the 3.4 Å resolution 2byq), which is positioned above (+) W147 and makes H-bonds to the backbone O of (–) I106 and backbone N of (–) I118 (*Ac* numbering).

2.2. Cross-docking structures

All AChBP structures co-crystallized with a non-toxin ligand (see Table 1), and the apo structure 2byn, were downloaded from the PDB, and the following dimers were used: 2byn-AE, 2wnl-AB, 2w8g-AB,DE,EA, 2pgz-AB, 2w8f-FG, 2wnj-AE, 2wn9-BC, 2byq-AB, 2bys-CD, 2byr-AB, 3c84-AB, 2wnc-DE, 1uv6-DE, 2zjv-AB, 1uw6-AB, 3c79-AB and 2zju-AB. The galanthamine–*Ac*-AChBP complex 2ph9 [11] was excluded because of weak ligand electron density. The ligand BDSAO in 2w8g displayed three different binding modes, all of which were included along with the corresponding dimers. Both alternate binding modes and corresponding binding site residue orientations of the 2wnj ligand DMXBA were used initially, however position A in the original PDB-file was preferred in all self, cross and ensemble dockings (results not shown) and hence is the one referred to throughout this paper.

Non-protein atoms, except the HOH1 water molecule defined in Section 2.1, were removed from each structure. All structures then were subjected to the Maestro built-in protein preparation protocol which adds hydrogen atoms and determines the protonation/tautomeric states of acidic and basic residues, probes the optimal flip orientation of glutamine, asparagine and histidine residues, optimizes H-bond networks, and finally performs a geometry optimization to a maximum RMSD of 0.3 Å. All prepared dimers were superimposed onto the 2byn-AE dimer using the protein structure alignment tool in Maestro, thus creating a common spatial reference frame to facilitate ligand heavy atoms RMSD measurements (see Section 2.4) in subsequent dockings. These dimers were used for cross-docking after adjusting residues (–) Q38 and (+) K143 (*Ac*-AChBP) to conformations matching those in 2byr, followed by a standard geometry optimization of only HOH1, with nicotine temporarily inserted in each binding pocket, in order to obtain correct H-bond directionality of HOH1. A set of duplicate structures of the *Ac*-AChBPs, in which (+) Y93 was given a conformation identical to that observed for lobeline in 2bys ($\chi_1 = 180^\circ$ instead of -70°), was generated as well for use in cross-docking in order to enable docking of lobeline in the correct binding mode in non-native receptors.

2.3. Ensemble generation

An ensemble of AChBP structures with systematically varying C-loop closures was generated for each species with the 2byn-AE (*Ac*) and 1uw6-AB (*Ls*) dimers, both including HOH1, as starting points. An iterative series of targeted molecular mechanics energy minimizations was performed (PRCG method with a gradient convergence threshold of 0.5 kJ/mol/Å) after the above described protein preparation procedure. During the energy minimizations, the distance between the C-loop tip centroid and the back wall centroid (defined in Section 2.1) was varied by applying distance constraints to this value. The concept is visualized for the *Ac* ensemble in Fig. 2. First, the initial value of this distance was kept to yield the first structure (19.7 Å for 2byn, 12.4 Å for 1uw6). The generated structure was used in the new minimization with the centroid-centroid target distance incremented/decremented by 1 Å, resulting in a model with a more open/closed C-loop which, in turn, was used in the next minimization with the target distance altered another 1 Å. Thus, each resulting model was used in an iterative manner as the starting point for the next minimization,

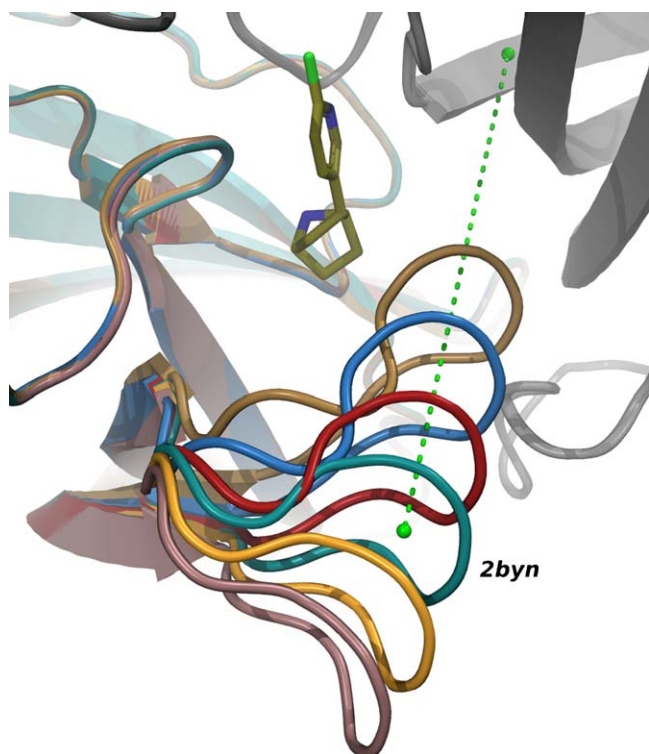


Fig. 2. Representative members of the conformational Ac ensemble generated by a consecutive series of geometry optimizations forcing the tip of the C-loop to move along the path (green dotted line) between the two defined centroids. Epibatidine is shown to highlight the binding site. Complementary (–) subunits are colored in gray. Principal (+) subunit coloring distinguish different degrees of C-loop closure. (Image generated with PyMOL [50]).

in total generating 17 models for each species (Ac and Ls). During the minimizations, tight ($10,000 \text{ kJ/mol/Å}^2$) constraints were used on the centroid-centroid distance, and the backwall centroid was anchored in space so that only the C-loop centroid was allowed to move. In order for the protein residues defining the centroids to follow the displacements, the same force constant was used to constrain them to remain within the initial distance to the corresponding centroid dummy atom. The generated models were subsequently aligned to the original 2byn-AE dimer and modified as described for the X-ray structures in the cross-docking experiment (HOH1 and, for Ac, residues (+) K143 and (–) Q38). Again, a duplicate Ac ensemble with (+) Y93 set to the “lobeline” conformation seen in 2bys was created.

2.4. Docking and pose evaluation

All ligands were built in their N-protonated state (except the neonicotinoids) by taking the coordinates from the crystal structure and subjecting them to a full geometry optimization with GB/SA solvation using the PRCG method converging to 0.05 kJ/mol/Å . Lobeline was put in an all-equatorial substituent chair conformation before minimization because its piperidine ring converges to an energetically unfavorable skew-boat when minimized directly from the crystal structure conformation. Anabaseine, although found in both its ammonium ketone and tetrahydropyridine forms in its crystal structure 2wnl, has been shown to be active as an nAChR agonist in its N-protonated tetrahydropyridine form [41] and hence is the one used here.

All binding pockets of crystal structures and ensemble members were defined in Glide by a $10 \text{ Å} \times 8 \text{ Å} \times 8 \text{ Å}$ box centered on the MLA ligand. The ligands were docked flexibly to ensemble members generated from the AChBP species in which it was crystal-

lized. Glide's Standard Precision scoring function was used without vdW scaling of receptor or ligand atoms, and five poses per ligand were requested in each docking. Two scoring functions in Glide were considered when ranking the docking poses, namely Gscore and Emodel [36]. Gscore, a modified and expanded version of the empirically based ChemScore [42], is fitted to reflect binding affinities (ΔG in kcal/mol) and is useful for rank ordering ligands in, e.g. a database screen. Emodel is a composite scoring function combining the Gscore, ligand–receptor molecular mechanics interaction energy, and ligand conformational strain, and was created for selecting the best docking pose for a ligand. Therefore, the Emodel score was used to internally rank the poses for each ligand in each separate docking, and the Gscore of the highest ranked pose was then used for comparison across dockings (i.e. across the different receptor structures).

The correctness of docking poses was assessed by comparing them to the crystal structures. Ligand heavy atoms RMSD values were calculated relative to geometry optimized versions of the X-ray structures. They were produced by a protein preparation run as described above in Section 2.2 with the modification that ligands and water molecules within 5 Å hereof were kept in the binding pocket throughout the protocol. The pyridine ring of epibatidine in the 2byq structure was rotated 180° to give it the same orientations as in the four other binding sites in that crystal structure (with 3.4 Å electron density resolution there is no evidence that in this particular binding pocket the ligand orientation should not be as the others, which in addition have the same pyridine orientation as the structurally similar nicotine). The amide group of carbamoylcholine was also flipped 180° in its X-ray structure (1uv6) to avoid the highly unfavorable conformation with electronic repulsion between the two oxygen atoms originally modeled into the electron density.

A docking pose with $\text{RMSD} \leq 2 \text{ Å}$ compared to the experimental structure was defined as correct. Poses of ca. $2\text{--}3.5 \text{ Å}$ were visually inspected to determine if they were to be considered correct or incorrect, with correct poses having the positively charged nitrogen in the aromatic box and an overall orientation similar to that seen in the X-ray structure. Examples of correct and incorrect poses are given in Supporting information.

3. Results and discussion

In the present study we focused our attention on the small molecule nAChR ligands co-crystallized with the AChBP. The structures and corresponding proteins considered are listed in Table 1. The C-loop closure (see definition above) of the included AChBP structures varies from 11.7 Å (3c84) up to 19.8 Å (2w8g), and for co-crystals with toxins it is up to 21.8 Å (2br8).

3.1. Cross-docking

Initially, a cross-docking study using Glide was conducted in order to: (1) assess the ability of Glide to reproduce the original binding modes of the ligands in the AChBP system; (2) verify that Glide's scoring algorithm is able to rank correct over incorrect receptor conformations for each ligand; (3) establish the optimal docking protocol; and (4) verify that self- and cross-docking was robust to conformational change of two peripheral residues (discussed further below). Table 1 summarizes the details of ligands, receptor structures, binding data, and docking results from the docking of all 15 ligands to all experimentally determined receptor structures. In addition to the 15 ligand bound complexes, the apo structure 2byn (C-loop closure: 19.7 Å) was included in the cross-docking because of its use in the subsequent ensemble generation.

As evident from the self-docking column in Table 1, Glide identifies the correct pose for each ligand in its native receptor and ranks

it as the best, with BDSAO (RMSD = 2.2 Å) and DDSAO (RMSD = 1.5 Å) deviating the most from the experimentally observed binding modes. In the original BDSAO crystal structure each of the three occupied binding sites displays a distinct binding mode, indicating that the ligand does not bind in a well defined manner and thus may be a difficult case for the docking program. DDSAO makes no direct H-bonds to the receptor, and the lack of such directional interactions apparently makes it difficult for Glide to obtain the experimentally observed binding mode. However, based on visual inspection we consider these binding modes qualitatively correct (examples of docking poses are given in [Supporting information](#)).

The cross-docking further confirms that Glide is generally able to award the best scores to ligands docked to either their native receptor or one with a similar C-loop closure, and all ligands except tropisetron obtain the best Gscore with a correct pose. Tropisetron scores marginally better in the cocaine-bound 2pgz than in its native 2wnc ([Table 1](#)), the two crystal structures having identical degrees of C-loop closure (14.0 and 14.1 Å, respectively). However, an RMSD of 3.9 Å for the 2pgz pose indicates that this ligand is a difficult case in non-native pockets. Glide favors a significant displacement of the indole-3-carboxylate moiety of tropisetron in non-native pockets relative to the observed binding mode in its native 2wnc due to markedly different conformations of (–) Y55 and (–) Q57. The same displacement can therefore be expected to dominate when docking to the Ac ensemble, which is based on a structure (2byn) with these residues in conformations similar to 2pgz.

Several settings in Glide were systematically varied in the cross-docking: scoring algorithm (standard (SP) or extra precision (XP)), vdW scaling of receptor and ligand atoms, use of ligand charges from force field (FF) or quantum mechanical (QM) calculations, and the use of post-docking minimization. Using the Glide SP scoring function, no vdW scaling, and including the Glide default post-docking minimization of poses in the pocket gave the results referred to here and were in best accordance with the observed binding modes (results from other combinations of settings are not shown). We therefore settled on this protocol for use in the subsequent ensemble docking. We further note that excluding vdW scaling is intuitively the optimal setting in our case. Reducing atom vdW radii is a general method for taking receptor flexibility into account, but in the present study this is handled explicitly through the use of conformational ensembles.

The final point of the cross-docking was concerned with residues (–) Q38 and (+) K143 (Ac), in the periphery of the binding pocket. MLA is the only ligand to reach both, and in its native structure, 2byr (Ac), they have a conformation distinct from those found in most (K143) or all (Q38) other X-ray structures. In the subsequent ensemble generation these residues had to be put in 2byr rotameric states in order to create a larger pocket for MLA to be docked correctly. Therefore, to validate that this would not impact the ability of Glide to correctly dock and score the other ligands, we conducted the cross-docking with all receptor pockets having these residues in 2byr rotameric states. Comparing the cross-docking results to those obtained in an identical experiment with the residues in their original state (not shown) gave no significant or systematic differences in pose accuracy or scoring, with the desired exception that MLA was only able to obtain correct and high scoring poses in the open-loop structures 2byn, 2w8f and 2w8g with the residues in altered states. This confirmed the validity of the approach taken in the ensemble docking, and indicated that MLA could be included in the study with satisfactory results.

An additional outcome of initial cross-docking experiments was the importance of including the water molecule HOH1 (defined previously) in the dockings. HOH1 donates an important H-bond to many ligands, e.g. the pyridine-N of nicotine, and is found in all

published AChBP structures where waters are modeled into the electron density (i.e. all except the 3.4 Å resolution 2byq). Preliminary dockings without HOH1 in place failed to consistently reproduce experimentally observed binding modes (results not shown). A GRID analysis of the 2byn-AE interface with the water probe confirmed the position of a tightly bound water molecule at this position with a predicted energy of –12.4 kcal/mol. Therefore, all receptor pockets in the cross-docking as well as in the ensemble docking included HOH1.

3.2. Ensemble generation

In the case of AChBP, and presumably also the nAChRs, variations occur in both side chain conformations and at the backbone level, and therefore both need to be considered in a docking protocol. Based on previous experience with generating ensembles of the ionotropic glutamate receptor [30], we first investigated if a coarse grained NMA method [43] suitable for describing large-scale flexibility in biomacromolecules could be applied to the AChBPs. The closing and opening motions of the C-loop are indeed captured by the slowest and most dominating normal modes, however important details of the backbone rotations playing a large part of the observed motion were lost because the method considers each residue a rigid block [44]. Therefore, with that method we were unable to reproduce the experimentally observed structures well enough for our purpose. MD based approaches may be better for this type of motions, since it explicitly simulates all atoms, bonds and torsions. Recently, such studies have been described for the AChBP [45] and for nAChR models [46] as well as other important drug targets such as the ACh esterase [47], avian influenza H5N1 neuraminidase [48], and the HIV-1 protease [29]. In our experience, drawbacks of MD as a method for ensemble generation include the rather time consuming steps needed in setting up, carrying out and analyzing the simulations properly, as well as the fact that the binding pockets often get distorted more than desired and thus prevents meaningful docking to the generated ensembles. Instead, we settled on a simplistic approach for generating conformational AChBP ensembles, namely the use of a series of constrained molecular mechanics structure optimizations forcing the tip of the C-loop to move closer to or away from the back wall of the binding pocket in a stepwise manner (see [Section 2](#) for details). Two 17-member ensembles, Ac and Ls, were generated, having C-loop closures ranging from extremely open (~24 Å for Ac, ~22 Å for Ls) to extremely closed (~9 Å).

A minimum requirement for a successful ensemble generation is that the less flexible side of the binding site does not drift throughout the consecutive structure optimizations. This was addressed by measuring heavy atom RMSD fits between each ensemble member and the starting structures for: (a) all pocket residues, and (b) non-C-loop pocket residues (i.e. excluding Ac residues (+) Q184-D197 or Ls residues (+) N181-D194). These data are given in [Fig. 3](#) and show the variation relative to the starting structure marked by an arrow in the figure. Comparing the V-shaped curves (all pocket residues) to the nearly flat curves (non-C-loop residues) it can be seen that the RMSD variation is almost solely attributable to the C-loop. Hence, no significant drift of the fixed part of the binding pockets are observed, which is also confirmed by visual inspection of the ensemble (note the invariance of the non-C-loop parts in [Fig. 2](#)). All models, except those with closures <10 Å, remain within 0.3 Å of the starting structure when considering only the non-C-loop part of the pocket ([Fig. 3](#), empty markers). The rise in RMSD for the extremely closed structures is observed because at that point the C-loop is forced further into the back wall of the pocket than would be physically feasible. At this point, the C-loop starts to clash sterically with residues on the complementary side of the binding

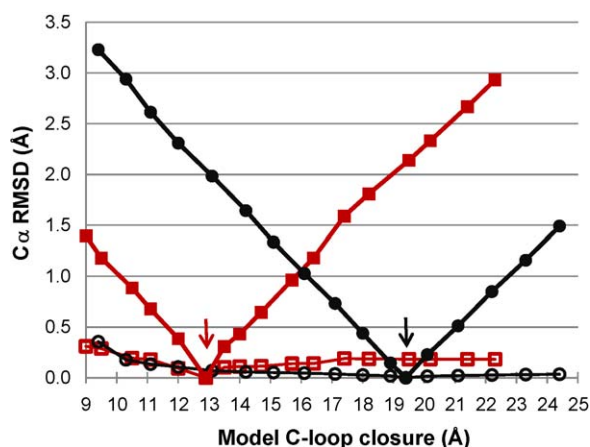


Fig. 3. Structural variation of the generated ensembles relative to the starting structures (marked by arrows), with the individual ensemble members represented by their C-loop closure. Ac-AChBP data are shown as black circles, and Ls-AChBP data are shown as red squares. For each ensemble, two C α RMSD fits for pocket residues are plotted against the C-loop closure, namely, (1) for all pocket residues (filled markers), and (2) for non-C-loop residues (empty markers). The RMSD values are measured after a least squares superposition of each ensemble member onto the corresponding starting structure using the appropriate pocket residues.

pocket, most notably Ls (–) W53 and M114, in turn perturbing the backbone slightly.

To validate the method in terms of being able to reproduce known intermediate structures, the binding pockets of the generated ensemble were compared to the crystal structures with the most similar C-loop closure. RMSD measurements show that the generated ensemble structures are as close to the crystal structures as crystal structures are to each other. The heavy atom RMSD deviations between ensemble structures and crystal structures are 0.5–1.4 Å, and by comparison, pairwise binding pocket RMSDs between representative crystal structures with similar C-loop closures fall in the ranges 0.6–1.4 Å.

Finally, we note that the ensemble generation procedure did not give rise to unfavorable backbone dihedral angles, i.e. no Ramachandran plot violations were observed (see [Supporting information](#)).

Together, these observations confirm that with the chosen method we were able to model a wide range of C-loop closures resulting in binding pocket structures which to a high degree of accuracy correspond to those seen in the experimentally determined crystal structures. We therefore conclude that the chosen method is suitable for generating a realistic structural ensemble with a high degree of control of and consistency in the conformational variation.

3.3. Ensemble docking

All 15 ligands were docked to each of the ensemble members in order to investigate if the docking score could be used to extract the correct ligand–receptor pairs, i.e. identify a correct pose of the ligand in a receptor with a C-loop closure resembling the experimentally observed one. The results are summarized in [Fig. 4](#), where the docking score (Gscore) of the highest ranked pose obtained in each model is plotted against the ensemble C-loop closure (for tabulated results see [Supporting information](#)).

In general, the docking scores follow a trend of decreasing (i.e. improving) values as the C-loop becomes more closed, until a point where the closure causes increasing values or no docking result at all. This corresponds well with what can be intuitively expected if the C-loop in a certain degree of closure results in the best possible fit to the ligand, while too open and closed con-

formations result in suboptimal interactions and steric clashes, respectively.

Fourteen, or 93%, of the ligands obtain the best Gscore in a model that has a C-loop closure within 2 Å of that observed in the corresponding X-ray structure, and for thirteen (87%) the predictions are within ~1 Å. This can be seen for each ligand in [Fig. 4](#) by comparing the C-loop closure giving rise to the best Gscore with the closure indicated by the dashed vertical line. BDSAO is the only ligand for which prediction of the ligand induced degree of C-loop closure fails completely with a deviation of 4–5 Å depending on which dimer interface of 2w8g is used for comparison.

In [Fig. 4](#) it is also indicated whether the top scoring docking poses are correct or incorrect compared to their experimental binding modes. Except for BDSAO, cocaine, tropisetron, and imidacloprid in the Ac but not in the Ls ensemble, all ligands dock correctly with their best scoring pose when using the RMSD and qualitative criteria described in Section 2 (examples of obtained poses compared to crystal structure binding modes are given in [Supporting information](#)).

In the search for an explanation for the failure of the four mentioned ligands to dock correctly, the ensemble docking results for these structures were carefully analyzed. As can be seen in [Fig. 4](#), BDSAO does obtain poses that we find correct in six of the seven models with the most open C-loops (RMSD = 3.1–3.3 Å relative to the 2w8g-EA crystal structure pose; see example in [Supporting information](#)). The relatively high RMSDs are due to a rotation of the dibenzosuberone moiety because (–) Y55 blocks part of the space that this bulky substituent fills in the crystal structure. In the Ac ensemble this residue has a different conformation than in 2w8g, both at the side chain and backbone levels. The same backbone flip and resulting ~120° χ_1 torsion rotation is also seen in other structures, including the tropisetron structure 2wnc as described for the cross-docking and further discussed below. This causes poorer Gscores (compare to the cross-docking data in [Table 1](#)) and thus results in incorrect poses (RMSD > 7 Å) in models with more closed C-loops.

In the four models with loop closures of 12–15 Å cocaine obtains the highest scores with similar poses, in which the tropane ring is rotated 180° to maintain the positive charge within the aromatic box while switching the positions of the two ester substituents compared to the crystal structure binding mode. This happens as a consequence of (–) Q57 having a slightly different position in 2byn, and hence in the entire Ac ensemble, relative to the X-ray structure 2pgz, which prevents the large benzyloxy moiety from being positioned in this region.

Like for cocaine, no correct binding modes were obtained for tropisetron in any ensemble member. As discussed in the cross-docking section, tropisetron was predicted to cause problems due to different orientations of residues (–) Q57 and (–) Y55 that caused Glide to favor poses with the indole-3-carboxylate moiety displaced downwards in the pocket, in turn forcing a 180° rotation of the tropane ring. This binding mode is top ranked in the five ensemble members with 12.0–16.1 Å C-loop closure, and despite deviating from the X-ray structure with RMSDs of 3.7–4.7 Å it is consistently close to the top ranked cross-docked poses in 2pgz (1.2–1.5 Å). Since Glide, as apparent from the cross-docking, slightly favors this binding mode over the experimentally observed, we cannot expect a different outcome from the ensemble docking, even if we used an additional Ac ensemble with the two mentioned residues in different rotameric states.

For the neonicotinoid imidacloprid, correct docking poses were almost exclusive to the Ls ensemble dockings, while a flipped orientation of the molecule was preferred in Ac in all but the most open model. We performed an additional QM/MM docking of imidacloprid using Schrödinger's QM-polarized ligand docking (QPLD) [49] module in order to investigate whether improved predictions

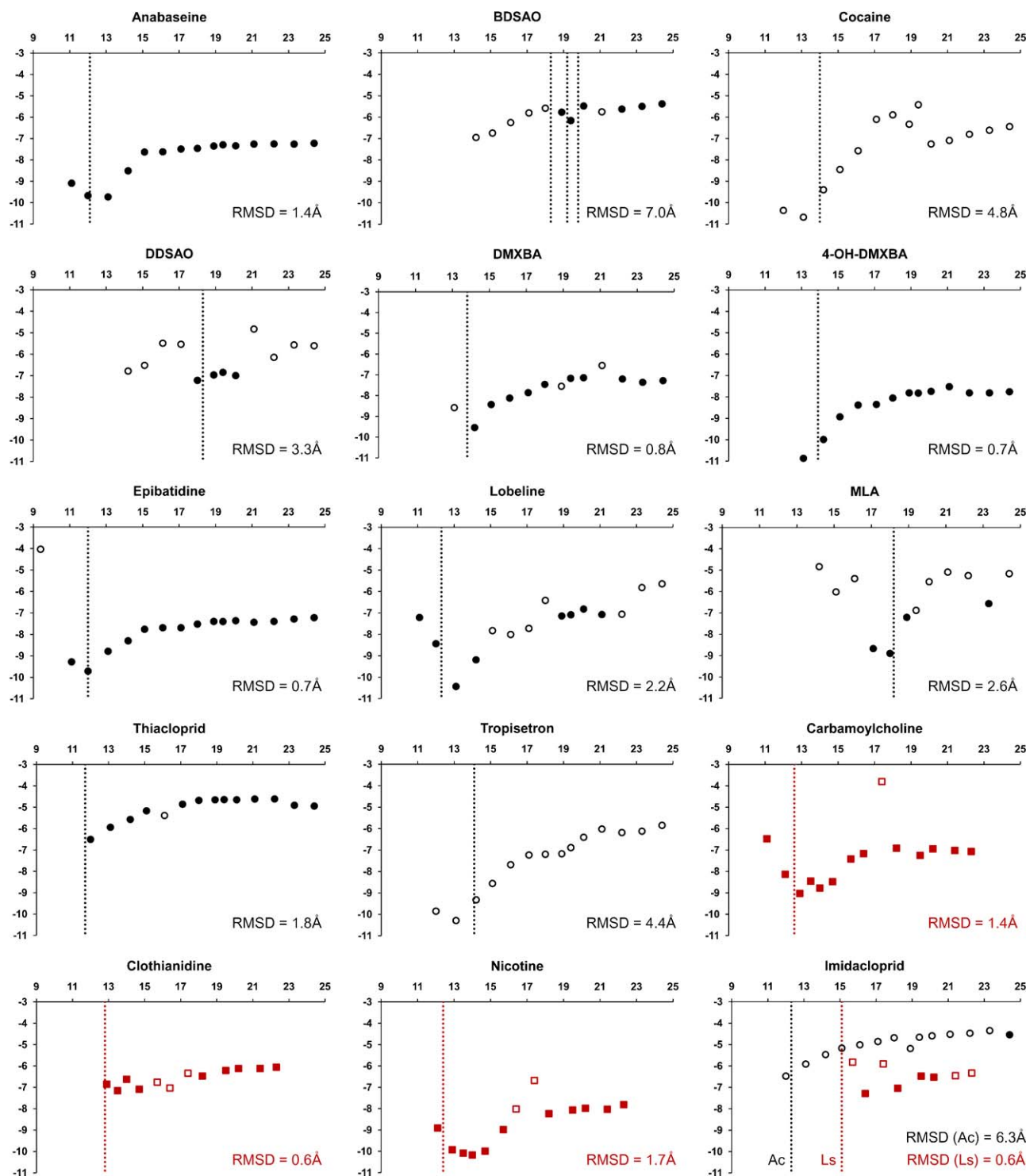


Fig. 4. Ensemble docking results. Y-axis: Gscore for the top ranking ligand pose in each ensemble member of the AChBP species in which it is crystallized; X-axis: C-loop closure in Å, representing the ensemble members. Black circles are for the Ac-AChBP ensemble, red squares for Ls-AChBP. Filled and empty markers indicate correct and incorrect docking poses, respectively. Results for lobeline are from the Ac-AChBP ensemble with (+) Y93 in the alternate ("lobeline") conformation. In each plot, the intersection of the vertical dashed line with the X-axis shows the C-loop closure observed in the corresponding ligand-AChBP complex X-ray structure (black and red indicate Ac and Ls, respectively). The three lines for BDSAO are due to three different binding modes in the same crystal structure giving rise to distinct closures. Heavy atom RMSDs are given for the overall best scoring pose for each ligand.

of the atomic charges would give better results (not shown). However, neither scores nor binding modes were significantly affected by this. Further, it should be noted that in the cross-docking similar flipped orientations of both imidacloprid and the closely related clothianidin were ranked near the top both in native and other pockets, thus indicating that minor differences in the pocket struc-

ture might tip the scale and favor the incorrect orientations. In spite of the described issues for imidacloprid, optimal Gscores are obtained in models with C-loop closures near or identical to those of its crystal structures.

Thus, issues with both the target structures and the docking algorithm seem to impact the ability to dock and score these com-

pounds in a consistently correct manner. It can be argued that the two mentioned residues, (–) Y55 and (–) Q57, could be accounted for explicitly, like we did for (–) Q38, (+) K143, and (+) Y93 in the *Ac* ensemble. Several factors speak against this. Firstly, Q38 and K143 differ from the others in that they were simply put in conformations that gave the largest possible space in the pocket to allow docking of the larger ligands (MLA in particular). The changes in rotameric states for the other three residues do not enlarge the pocket as such, but rather they free space in one area of the pocket and block another. While Y93 in the core of the binding pocket displays a simple change in its χ_1 torsion between the “lobeline” (2bys) conformation and the one seen in the other X-ray structures, the change observed for Y55 is more subtle in that it involves the backbone as well. Such an alteration would require the use of another structure as basis for the ensemble generation, which would add a great amount of complexity to the study. As for Q57, this peripheral residue probably could have been accounted for in a manner similar to Y93, although it displays a larger degree of variation. We deliberately chose not to introduce additional complexity into the study. The Y93 change was only included as a test case in order to establish that lobeline could be accurately accounted for. Expanding the study to account for all observed residue flexibilities in the periphery of the pocket would, in addition to the mentioned residues, require specific alterations for (–) M115, (–) S167, (+) Q186 and (+) S189, something that would be beyond the scope of the study. It should be mentioned that methods have been developed to model such changes at the individual side chain level, e.g. Schrödinger's Induced Fit Docking [26].

Our results thus highlight the crucial influence that both minor differences in individual residue positions as well as large-scale conformational states have on the ability to successfully carry out a docking protocol.

The issues with handling protein flexibility (both on smaller and larger scale) are well known, and in that context it is encouraging that the above comparison of the ensemble docking results with the experimentally determined X-ray structures shows that it is feasible to model large scale protein flexibility (in this case loop movement) by the approach described here. Not only is it possible to generate the relevant loop closure, but it is also possible to identify the most relevant member of the ensemble (based on the docking score), and in most cases even correct binding modes are reproduced. This analysis paves the way for using this type of protein ensemble generation in, e.g. virtual screening. Using an ensemble for a virtual screening would normally introduce more noise than signal. However, because our results indicate that the best docking score is obtained in the ensemble member with the most relevant C-loop closure, it is more probable that the ligand/protein combination selected using the docking score is the most relevant, and thus it is more probable that one can filter away the noise generated by docking into an ensemble.

The above analysis is in itself mostly of methodological interest, because the AChBPs are not of any particular interest *per se*. Nonetheless, the results point to the use of ensemble docking particularly for homology models of nAChRs or other Cys-loop receptors (which are of broader interest), because the analysis demonstrates that large scale protein movements can be modeled satisfactorily in Cys-loop receptors.

4. Conclusions

In the present study we have used the AChBP as a model for nAChRs to evaluate a docking protocol allowing for explicit consideration of flexibility of the C-loop known to close in as a lid upon ligand binding. C-loop flexibility was modeled from a single AChBP

structure with a series of geometry optimizations targeting the C-loop to move closer to or away from a specified reference point. This allowed for a high degree of control over the process, resulting in the generation of a set of conformers with gradual and consistent changes in the C-loop and hence in the size of the binding pocket. While a certain distance between the C-loop and the reference point (the ‘back wall centroid’) was enforced, the actual trajectory was determined by the minimum energy pathway needed to travel in order to satisfy the constraint. With the method, known experimental structures of the AChBP along the trajectory were reproduced as close as can be expected when also considering the small differences that exist between crystal structures with similar degrees of C-loop closure.

Based on cross-docking of each of the investigated ligands to all experimentally determined proteins, a docking protocol involving flexible ligand docking, no vdW scaling and post-docking minimization of the ligand was identified as giving the best results and additionally confirmed that the correct receptor ligand pairs could be identified based on the docking score alone. Subsequent docking of all ligands to the conformational ensemble generated by constrained geometry optimizations resulted in identification of the correct degree of C-loop closure in 14 out of 15 and the correct binding mode in 12 out of 15 cases. This indicates that the generated ensembles can be useful for screening for new potential nAChR ligands, either in the AChBP directly, or in homology models based on AChBP. Furthermore, the method has the potential not only to pick out compounds with nAChR affinity from a database but to establish a hypothesis of which conformational changes it induces in the binding pocket. Induced C-loop closure has been proposed to at least partially determine the functional profile of an nAChR ligand [9], and hence its prediction could provide an early filter that increases the probability of filtering out compounds with the desired functional property.

Acknowledgements

The Carlsberg Foundation and the Lundbeck Foundation are gratefully acknowledged for financial support.

Appendix A. Supplementary data

Supplementary data associated with this article can be found, in the online version, at doi:10.1016/j.jmgm.2010.08.004.

References

- [1] A.A. Jensen, B. Frølund, T. Liljefors, P. Krogsgaard-Larsen, Neuronal nicotinic acetylcholine receptors: structural revelations, target identifications, and therapeutic inspirations, *J. Med. Chem.* 48 (2005) 4705–4745.
- [2] N. Unwin, Refined structure of the nicotinic acetylcholine receptor at 4 Å resolution, *J. Mol. Biol.* 346 (2005) 967–989.
- [3] C.D. Dellisanti, Y. Yao, J.C. Stroud, Z.Z. Wang, L. Chen, Crystal structure of the extracellular domain of nAChR $\alpha 1$ bound to α -bungarotoxin at 1.94 Å resolution, *Nat. Neurosci.* 10 (2007) 953–962.
- [4] K. Brejc, W.J. van Dijk, R.V. Klaassen, M. Schuurmans, J. van der Oost, A.B. Smit, T.K. Sixma, Crystal structure of an ACh-binding protein reveals the ligand-binding domain of nicotinic receptors, *Nature* 411 (2001) 269–276.
- [5] P.H. Celie, S.E. van Rossum-Fikkert, W.J. van Dijk, K. Brejc, A.B. Smit, T.K. Sixma, Nicotine and carbamylcholine binding to nicotinic acetylcholine receptors as studied in AChBP crystal structures, *Neuron* 41 (2004) 907–914.
- [6] Y. Bourne, T.T. Talley, S.B. Hansen, P. Taylor, P. Marchot, Crystal structure of a Cbtx-AChBP complex reveals essential interactions between snake α -neurotoxins and nicotinic receptors, *EMBO J.* 24 (2005) 1512–1522.
- [7] P.H. Celie, R.V. Klaassen, S.E. van Rossum-Fikkert, E.R. van, N.P. van, A.B. Smit, T.K. Sixma, Crystal structure of acetylcholine-binding protein from *Bulinus truncatus* reveals the conserved structural scaffold and sites of variation in nicotinic acetylcholine receptors, *J. Biol. Chem.* 280 (2005) 26457–26466.
- [8] P.H. Celie, I.E. Kasheverov, D.Y. Mordvintsev, R.C. Hogg, N.P. van, E.R. van, S.E. van Rossum-Fikkert, M.N. Zhmak, D. Bertrand, V. Tsetlin, T.K. Sixma, A.B. Smit, Crystal structure of nicotinic acetylcholine receptor homolog AChBP in complex with an α -conotoxin PnIA variant, *Nat. Struct. Mol. Biol.* 12 (2005) 582–588.

- [9] S.B. Hansen, G. Sulzenbacher, T. Huxford, P. Marchot, P. Taylor, Y. Bourne, Structures of Aplysia AChBP complexes with nicotinic agonists and antagonists reveal distinctive binding interfaces and conformations, *EMBO J.* 24 (2005) 3635–3646.
- [10] C. Ulens, R.C. Hogg, P.H. Celie, D. Bertrand, V. Tsetlin, A.B. Smit, T.K. Sixma, Structural determinants of selective α -conotoxin binding to a nicotinic acetylcholine receptor homolog AChBP, *Proc. Natl. Acad. Sci. U.S.A.* 103 (2006) 3615–3620.
- [11] S.B. Hansen, P. Taylor, Galanthamine and non-competitive inhibitor binding to ACh-binding protein: evidence for a binding site on non- α -subunit interfaces of heteromeric neuronal nicotinic receptors, *J. Mol. Biol.* 369 (2007) 895–901.
- [12] S. Dutertre, C. Ulens, R. Buttner, A. Fish, E.R. van, Y. Kendel, G. Hopping, P.F. Alewood, C. Schroeder, A. Nicke, A.B. Smit, T.K. Sixma, R.J. Lewis, AChBP-targeted α -conotoxin correlates distinct binding orientations with nAChR subtype selectivity, *EMBO J.* 26 (2007) 3858–3867.
- [13] M. Ihara, T. Okajima, A. Yamashita, T. Oda, K. Hirata, H. Nishiwaki, T. Morimoto, M. Akamatsu, Y. Ashikawa, S. Kuroda, R. Mega, S. Kuramitsu, D. Sattelle, K. Matsuda, Crystal structures of *Lymanaea stagnalis* AChBP in complex with neonicotinoid insecticides imidacloprid and clothianidin, *Invert. Neurosci.* 8 (2008) 71–81.
- [14] T.T. Talley, M. Harel, R.E. Hibbs, Z. Radic, M. Tomizawa, J.E. Casida, P. Taylor, Atomic interactions of neonicotinoid agonists with AChBP: molecular recognition of the distinctive electronegative pharmacophore, *Proc. Natl. Acad. Sci. U.S.A.* 105 (2008) 7606–7611.
- [15] C. Ulens, A. Akdemir, A. Jongejan, R. van Elk, S. Bertrand, A. Perrakis, R. Leurs, A.B. Smit, T.K. Sixma, D. Bertrand, I.J.P. de Esch, Use of acetylcholine binding protein in the search for novel $\alpha 7$ nicotinic receptor ligands. In silico docking, pharmacological screening, and X-ray analysis, *J. Med. Chem.* 52 (2009) 2372–2383.
- [16] R.E. Hibbs, G. Sulzenbacher, J. Shi, T.T. Talley, S. Conrod, W.R. Kem, P. Taylor, P. Marchot, Y. Bourne, Structural determinants for interaction of partial agonists with acetylcholine binding protein and neuronal $\alpha 7$ nicotinic acetylcholine receptor, *EMBO J.* 28 (2009) 3040–3051.
- [17] D.A. Dougherty, Cys-loop neuroreceptors: structure to the rescue? *Chem. Rev.* 108 (2008) 1642–1653.
- [18] S.B. Hansen, Z. Radic, T.T. Talley, B.E. Molles, T. Deerinck, I. Tsigelny, P. Taylor, Tryptophan fluorescence reveals conformational changes in the acetylcholine binding protein, *J. Biol. Chem.* 277 (2002) 41299–41302.
- [19] H.M. Berman, J. Westbrook, Z. Feng, G. Gilliland, T.N. Bhat, H. Weissig, I.N. Shindyalov, P.E. Bourne, The Protein Data Bank, *Nucleic Acids Res.* 28 (2000) 235–242.
- [20] A.B. Smit, N.I. Syed, D. Schaap, M.J. van, J. Klumperman, K.S. Kits, H. Lodder, R.C. van der Schors, E.R. van, B. Sorgedrag, K. Brejc, T.K. Sixma, W.P. Geraerts, A glia-derived acetylcholine-binding protein that modulates synaptic transmission, *Nature* 411 (2001) 261–268.
- [21] R.J. Law, R.H. Henchman, J.A. McCammon, A gating mechanism proposed from a simulation of a human $\alpha 7$ nicotinic acetylcholine receptor, *Proc. Natl. Acad. Sci. U.S.A.* 102 (2005) 6813–6818.
- [22] X. Cheng, H. Wang, B. Grant, S.M. Sine, J.A. McCammon, Targeted molecular dynamics study of C-loop closure and channel gating in nicotinic receptors, *PLoS Comput. Biol.* 2 (2006) e134.
- [23] X. Cheng, I. Ivanov, H. Wang, S.M. Sine, J.A. McCammon, Nanosecond-timescale conformational dynamics of the human $\alpha 7$ nicotinic acetylcholine receptor, *Biophys. J.* 93 (2007) 2622–2634.
- [24] P. Tosco, P.K. Ahling, T. Dyhring, D. Peters, K. Harpsøe, T. Liljefors, T. Balle, Complementary three-dimensional quantitative structure–activity relationship modeling of binding affinity and functional potency: a study on $\alpha 4\beta 2$ nicotinic ligands, *J. Med. Chem.* 52 (2009) 2311–2316.
- [25] V. Mohan, A.C. Gibbs, M.D. Cummings, E.P. Jaeger, R.L. Desjarlais, Docking: successes and challenges, *Curr. Pharm. Des.* 11 (2005) 323–333.
- [26] W. Sherman, T. Day, M.P. Jacobson, R.A. Friesner, R. Farid, Novel procedure for modeling ligand/receptor induced fit effects, *J. Med. Chem.* 49 (2006) 534–553.
- [27] H.B. Broughton, A method for including protein flexibility in protein–ligand docking: improving tools for database mining and virtual screening, *J. Mol. Graph. Model.* 18 (2000) 247–257.
- [28] H.A. Carlson, K.M. Masukawa, K. Rubins, F.D. Bushman, W.L. Jorgensen, R.D. Lins, J.M. Briggs, J.A. McCammon, Developing a dynamic pharmacophore model for HIV-1 integrase, *J. Med. Chem.* 43 (2000) 2100–2114.
- [29] K.L. Meagher, H.A. Carlson, Incorporating protein flexibility in structure-based drug discovery: using HIV-1 protease as a test case, *J. Am. Chem. Soc.* 126 (2004) 13276–13281.
- [30] T. Sander, T. Liljefors, T. Balle, Prediction of the receptor conformation for iGluR2 agonist binding: QM/MM docking to an extensive conformational ensemble generated using normal mode analysis, *J. Mol. Graph. Model.* 26 (2008) 1259–1268.
- [31] C.N. Cavasotto, J.A. Kovacs, R.A. Abagyan, Representing receptor flexibility in ligand docking through relevant normal modes, *J. Am. Chem. Soc.* 127 (2005) 9632–9640.
- [32] N. Floquet, J.D. Marechal, M.A. Badet-Denisot, C.H. Robert, M. Dauchez, D. Perahia, Normal mode analysis as a prerequisite for drug design: application to matrix metalloproteinases inhibitors, *FEBS Lett.* 580 (2006) 5130–5136.
- [33] K.L. Damm, H.A. Carlson, Exploring experimental sources of multiple protein conformations in structure-based drug design, *J. Am. Chem. Soc.* 129 (2007) 8225–8235.
- [34] Maestro, Version 8.5, Schrödinger, LLC, New York, NY, 2008.
- [35] Glide, Version 5.0, Schrödinger, LLC, New York, NY, 2008.
- [36] R.A. Friesner, J.L. Banks, R.B. Murphy, T.A. Halgren, J.J. Klicic, D.T. Mainz, M.P. Repasky, E.H. Knoll, M. Shelley, J.K. Perry, D.E. Shaw, P. Francis, P.S. Shenkin, Glide: a new approach for rapid, accurate docking and scoring. 1. Method and assessment of docking accuracy, *J. Med. Chem.* 47 (2004) 1739–1749.
- [37] T.A. Halgren, R.B. Murphy, R.A. Friesner, H.S. Beard, L.L. Frye, W.T. Pollard, J.L. Banks, Glide: a new approach for rapid, accurate docking and scoring. 2. Enrichment factors in database screening, *J. Med. Chem.* 47 (2004) 1750–1759.
- [38] MacroModel, Version 9.6, Schrödinger, LLC, New York, NY, 2008.
- [39] GRID, Version 22a, Molecular Discovery, Ltd., Pinner, Middlesex, 2005.
- [40] P.J. Goodford, A computational procedure for determining energetically favorable binding sites on biologically important macromolecules, *J. Med. Chem.* 28 (1985) 849–857.
- [41] W.R. Kem, V.M. Mahnir, L.B. Bloom, B.J. Gabrielson, The active form of the nicotinic receptor agonist anabaseine is the cyclic iminium cation, *Toxicol.* 33 (1995) 306.
- [42] M.D. Eldridge, C.W. Murray, T.R. Auton, G.V. Paolini, R.P. Mee, Empirical scoring functions: I. The development of a fast empirical scoring function to estimate the binding affinity of ligands in receptor complexes, *J. Comput. Aided Mol. Des.* 11 (1997) 425–445.
- [43] W. Zheng, S. Doniach, A comparative study of motor-protein motions by using a simple elastic-network model, *Proc. Natl. Acad. Sci. U.S.A.* 100 (2003) 13253–13258.
- [44] T. Sander, Unpublished work, 2009.
- [45] F. Gao, N. Bern, A. Little, H.L. Wang, S.B. Hansen, T.T. Talley, P. Taylor, S.M. Sine, Curariform antagonists bind in different orientations to acetylcholine-binding protein, *J. Biol. Chem.* 278 (2003) 23020–23026.
- [46] J. Sgrignani, C. Bonaccini, G. Grazioso, M. Chioccioli, A. Cavalli, P. Gratter, Insights into docking and scoring neuronal $\alpha 4\beta 2$ nicotinic receptor agonists using molecular dynamics simulations and QM/MM calculations, *J. Comput. Chem.* 30 (2009) 2443–2454.
- [47] J. Kua, Y. Zhang, A.C. Eslami, J.R. Butler, J.A. McCammon, Studying the roles of W86, E202, and Y337 in binding of acetylcholine to acetylcholinesterase using a combined molecular dynamics and multiple docking approach, *Protein Sci.* 12 (2003) 2675–2684.
- [48] R.E. Amaro, D.D.L. Minh, L.S. Cheng, W.M. Lindstrom, A.J. Olson, J.H. Lin, W.W. Li, J.A. McCammon, Remarkable loop flexibility in avian influenza N1 and its implications for antiviral drug design, *J. Am. Chem. Soc.* 129 (2007) 7764–7765.
- [49] Schrödinger Suite 2008 QM-Polarized Ligand Docking protocol; Glide version 5.0, Schrödinger, LLC, New York, NY, 2008; Jaguar version 7.5, Schrödinger, LLC, New York, NY, 2008; QSite version 5.0, Schrödinger, LLC, New York, NY, 2008.
- [50] The PyMOL Molecular Graphics System, Version 1.2r2, DeLano Scientific, Palo Alto, CA, USA, 2009.
- [51] T.T. Talley, S. Yalda, K.Y. Ho, Y. Tor, F.S. Soti, W.R. Kem, P. Taylor, Spectroscopic analysis of benzylidene anabaseine complexes with acetylcholine binding proteins as models for ligand–nicotinic receptor interactions, *Biochemistry* 45 (2006) 8894–8902.
- [52] S.B. Hansen, T.T. Talley, Z. Radic, P. Taylor, Structural and ligand recognition characteristics of an acetylcholine-binding protein from *Aplysia californica*, *J. Biol. Chem.* 279 (2004) 24197–24202.